Ferrocene-Promoted Photoactivated DNA Cleavage and Anticancer Activity of Terpyridyl Copper(II) Phenanthroline Complexes

ARTICLE *in* ORGANOMETALLICS · JULY 2010

Impact Factor: 4.13 · DOI: 10.1021/om100524x · Source: OAI

3632 *Organometallics* **2010,** *29,* 3632–3641
DOI: 10.1021/om100524x

ORGANOMETALLICS
Article

Ferrocene-Promoted Photoactivated DNA Cleavage and Anticancer Activity of Terpyridyl Copper(II) Phenanthroline Complexes

Basudev Maity,[†] Mithun Roy,[†] Bhabatosh Banik,[†] Ritankar Majumdar,[‡] Rajan R. Dighe,[‡] and Akhil R. Chakravarty*,[†]

[†]*Department of Inorganic and Physical Chemistry,* [‡]*Department of Molecular Reproduction, Development and Genetics, Indian Institute of Science, Bangalore 560012, India*

Received May 28, 2010

Ferrocene-appended copper(II) complexes $[Cu(Fc\text{-}tpy)(B)](ClO_4)_2$ (**1**−**3**) and $[Cu(Ph\text{-}tpy)(dppz)](ClO_4)_2$ (**4**) as control, where Fc-tpy is 4′-ferrocenyl-2,2′:6′,2″-terpyridine, Ph-tpy is 4′-phenyl-2,2′:6′,2″-terpyridine, and B is a phenanthroline base, viz., 1,10-phenanthroline (phen, **1**), dipyridoquinoxaline (dpq, **2**), and dipyridophenazine (dppz, **3**), were prepared and structurally characterized, and their DNA binding, photoactivated DNA cleavage activity, and cytotoxic properties were studied [Fc = $(\eta^5\text{-}C_5H_4)Fe^{II}(\eta^5\text{-}C_5H_5)$]. Complexes **1** and **3** as hexafluorophosphate salts were structurally characterized by X-ray crystallography. Molecular structures of $[Cu(Fc\text{-}tpy)(phen)](PF_6)_2$ (**1a**) and $[Cu(Fc\text{-}tpy)(dppz)](PF_6)_2\cdot MeCN$ (**3a**·MeCN) show a distorted square-pyramidal geometry at copper(II), with the Fc-tpy ligand and the phenanthroline base showing respective tridentate and bidentate binding modes. The phenanthroline base exhibits axial−equatorial bonding, while the Fc-tpy ligand binds at the basal plane. The complexes showed quasi-reversible cyclic voltammetric responses near 0.45 and −0.3 V vs SCE in aqueous DMF−0.1 M KCl assignable to the Fc^+−Fc and Cu(II)−Cu(I) redox couples, respectively. The complexes bind to DNA, giving K_b values of 1.4×10^4 to 5.6×10^5 M^{-1} in the order **4** ∼ **3** > **2** > **1**. Thermal denaturation and viscometric titration data suggest groove and/or partial intercalative mode of DNA binding of the complexes. The complexes showed chemical nuclease activity in the presence of 3-mercaptopropionic acid (0.5 mM) or H_2O_2 (0.25 mM). Complexes **2**−**4** showed plasmid DNA cleavage activity in visible light, forming $^{\bullet}OH$ radicals. The Fc-tpy complex **3** showed better DNA photocleavage activity than its Ph-tpy analogue. The ferrocene moiety in the dppz complex **3** makes it more photocytotoxic than the Ph-tpy analogue **4** in HeLa cells.

Introduction

Transition metal complexes showing anticancer activity have been extensively studied following the discovery of cisplatin and its analogues as transcription inhibitors.[1−8] The inherent dark toxicity and cellular resistivity have generated subsequent interest to develop a new generation of platinum-based anticancer agents. Lippard and co-workers have recently reported Pt(IV) prodrugs that could generate cisplatin on intracellular reduction of the metal.[9] An alternate strategy could be to design organometallic compounds that are suitable as anticancer agents, as exemplified by titanocene dichloride, ferrocifen, and half-sandwich (arene)ruthenium complexes.[10−14] Ferrocene, with its significant lipophilicity, could result in better cell permeability and stability in biological aqueous medium, and its reversible redox property makes it suitable for designing ferrocene-based bioorganometallic species for therapeutic applications.[11,15−17] For example, the ferrocenyl moiety in ferrocifen, which is a ferrocene-conjugated tamoxifen, significantly augments the anticancer activity of tamoxifen.[11] Ferrocene itself is not cytotoxic, and it

*To whom correspondence should be addressed. Fax: 91-80-23600683. E-mail: arc@ipc.iisc.ernet.in.

(1) Rosenberg, B.; van Camp, L.; Trosko, J. E.; Mansour, V. H. *Nature* **1969**, *222*, 385–386.
(2) Jung, Y.; Lippard, S. J. *Chem. Rev.* **2007**, *107*, 1387–1407.
(3) Guo, Z.; Sadler, P. J. *Angew. Chem., Int. Ed.* **1999**, *38*, 1512–1531.
(4) Reedijk, J. *Eur. J. Inorg. Chem.* **2009**, 1303–1312.
(5) Galanski, M.; Keppler, B. *Anti-cancer Agents in Med. Chem.* **2007**, *7*, 55–73.
(6) Kelland, L. *Nat. Rev. Cancer* **2007**, *7*, 573–584.
(7) Mao, J.; Zhang, Y.; Zhu, J.; Zhang, C.; Guo, Z. *Chem. Commun.* **2009**, 908–910.
(8) Singh, T. N.; Turro, C. *Inorg. Chem.* **2004**, *43*, 7260–7262.
(9) (a) Dhar, S.; Lippard, S. J. *Proc. Natl. Acad. Sci. U. S. A.* **2009**, *106*, 22199–22204. (b) Dhar, S.; Liu, Z.; Thomale, J.; Dai, H.; Lippard, S. J. *J. Am. Chem. Soc.* **2008**, *130*, 11467–11476. (c) Lovejoy, K. S.; Lippard, S. J. *Dalton Trans.* **2009**, 10651–10659.
(10) Köpf-Maier, P. *Anticancer Res.* **1999**, *19*, 493–504.
(11) Jaouen, G.; Top, S.; Vessires, A.; Leclercq, G.; McGlinchey, M. J. *Curr. Med. Chem.* **2004**, *11*, 2505–2517.
(12) Peacock, A. F. A.; Sadler, P. J. *Chem. Asian J.* **2008**, *3*, 1890–1899.
(13) Bergamo, A.; Sava, G. *Dalton Trans.* **2007**, 1267–1272.
(14) (a) Allardyce, C. S.; Dorcier, A.; Scolaro, C.; Dyson, P. J. *Appl. Organomet. Chem.* **2005**, *19*, 1–10. (b) Hartinger, C. G.; Dyson, P. J. *Chem. Soc. Rev.* **2009**, *38*, 391–401.
(15) Van Staveren, D. R.; Metzler-Nolte, N. *Chem. Rev.* **2004**, *104*, 5931–5985.
(16) Fouda, M. F. R.; Abd-Elzaher, M. M.; Abdelsamaia, R. A.; Labib, A. A. *Appl. Organomet. Chem.* **2007**, *21*, 613–625.
(17) Swarts, J. C.; Vosloo, T. G.; Cronje, S. J.; Du Plessis, W. C.; Van Rensburg, C. E. J.; Kreft, E.; Van Lier, J. E. *Anticancer Res.* **2008**, *28*, 2781–2784.

 Published on Web 07/20/2010

does not show much antitumor activity. However, the ferrocenium cation, which is a one-electron oxidized product of ferrocene, is known to show cytotoxic activity.[18,19] Osella and co-workers have reported the cytotoxicity of ferrocenium cationic salts showing oxidative DNA damage.[18] Since the ferrocenium cation generally degrades in biological aqueous medium, functionalization of the aromatic ring(s) could give stability to the ferrocenium cation. The present work stems from our interest in designing ferrocene-conjugated terpyridyl copper(II) complexes, which is expected to generate a reactive ferrocenium cationic moiety on photoactivation in visible light, while the complex remains inactive in the dark. The objective of using the terpyridyl copper(II) moiety is to enhance the photooxidation propensity of ferrocene. The presence of metal-bound planar phenanthroline bases as binders to double-stranded DNA could facilitate the hydrogen atom abstraction from the sugar unit. The objective for using the copper(II) ion in the structure is to have a visible spectral band within the photodynamic therapy (PDT) window of 620−850 nm to observe desired photoactivated DNA cleavage activity in red light.

The concept of photoactivated chemotherapy using transition metal complexes originates from the PDT of cancer in which a PDT drug, viz., the hematoporphyrin species Photofrin, on photoactivation at its lowest energy Q-band of 630 nm generates $^1\pi\pi^*$ state with subsequent formation of a $^3\pi\pi^*$ state that activates molecular oxygen from its stable triplet ($^3O_2$) to the reactive singlet state ($^1O_2$) by energy transfer in a type II pathway.[20−22] The porphyrin-based drugs suffer from skin toxicity and hepatotoxicity.[23] Phthalocyanine and other organic dyes have been extensively studied for their utility as PDT agents as substitutes of Photofrin.[24,25] The efficacy of organic dyes following type II pathway as PDT agents depends on their ability to generate singlet oxygen species.[26] Transition metal complexes with their versatile coordination geometry and spectral, magnetic, and redox properties could provide alternate pathways such as a photoredox or type- I pathway to generate reactive species, damaging DNA.[27] The chemistry of metal-based photochemotherapeutic agents is of recent origin.[28−32] While transition metal-based complexes having low-energy charge transfer or d−d band(s) are known to show DNA photocleavage activity in visible light, there are only a few reports available on organometallic complexes showing similar DNA cleavage activity in UV light or visible light of high energy.[33−38] Half-sandwich organometallic complexes of iron and tungsten are also known to show photoinduced DNA cleavage activity in UV light via photogenerated methyl radicals.[33]

We have recently shown that ferrocene-appended copper(II) complexes having a tripodal ligand or amino acid-reduced Schiff base and phenanthroline bases act as multifunctional model nucleases.[39,40] In continuation of our efforts to explore this chemistry further, we have now synthesized ferrocene-appended terpyridyl copper(II) complexes having phenanthroline bases and studied their photoactivated DNA cleavage property. The terpyridine ligand with its pyridyl moiety bound to Fc is likely to significantly enhance the DNA cleavage activity by formation of reactive ferrocenium species [Fc = (η^5-C_5H_4)Fe^{II}(η^5-C_5H_5)]. Herein, we present the synthesis, structure, and DNA binding and photoinduced DNA cleavage activity of the ferrocene-appended terpyridyl copper(II) complexes [Cu(Fc-tpy)(B)]$(ClO_4)_2$ (**1**−**3**), where Fc-tpy is 4′-ferrocenyl-2,2′:6′,2″-terpyridine and B is a N,N-donor heterocyclic base, namely, 1,10-phenanthroline (phen in **1**), dipyrido[3,2-*d*:2′,3′-*f*]quinoxaline (dpq in **2**), and dipyrido[3,2-*a*:2′,3′-*c*]phenazine (dppz in **3**) (Chart 1). To explore the effect of the ferrocenyl moiety on the overall DNA cleavage activity and photocytotoxicity, we have prepared and studied [Cu(Ph-tpy)(dppz)]$(ClO_4)_2$ (**4**) as a control species, where Ph-tpy is 4′-phenyl-2,2′:6′,2″-terpyridine. Complexes **1** and **3** as hexafluorophosphate salts have been structurally characterized by X-ray crystallography. We have observed significant enhancement in the visible light-induced DNA cleavage activity and cytotoxicity of the ferrocene-appended copper(II) complex over the control species, which lacks the ferrocenyl moiety.

Results and Discussion

Synthesis and General Aspects. Copper(II) complexes [Cu(Fc-tpy)(B)]$(ClO_4)_2$ (**1**−**3**) were synthesized in good yield

(18) Tabbì, G.; Cassino, C.; Cavigiolio, G.; Colangelo, D.; Ghiglia, A.; Viano, I.; Osella, D. *J. Med. Chem.* **2002**, *45*, 5786–5796.
(19) Osella, D.; Ferrali, M.; Zanello, P.; Laschi, F.; Fontani, M.; Nervi, C.; Cavigiolio, G. *Inorg. Chim. Acta* **2000**, *306*, 42–48.
(20) Bonnett, R. *Chemical Aspects of Photodynamic Therapy*; Gordon & Breach: London, U.K., 2000.
(21) Henderson, B. W.; Busch, T. M.; Vaughan, L. A.; Frawley, N. P.; Babich, D.; Sosa, T. A.; Zollo, J. D.; Dee, A. S.; Cooper, M. T.; Bellnier, D. A.; Greco, W. R.; Oseroff, A. R. *Cancer Res.* **2000**, *60*, 525–529.
(22) Detty, M. R.; Gibson, S. L.; Wagner, S. J. *J. Med. Chem.* **2004**, *47*, 3897–3915.
(23) (a) Ochsner, M. *J. Photochem. Photobiol. B* **1996**, *32*, 3–9. (b) Moriwaki, S. I.; Misawa, J.; Yoshinari, Y.; Yamada, I.; Takigawa, M.; Tokura, Y. *Photodermatol. Photoimmunol. Photomed.* **2001**, *17*, 241–243.
(24) Sessler, J. L.; Hemmi, G.; Mody, T. D.; Murai, T.; Burrell, A.; Young, S. W. *Acc. Chem. Res.* **1994**, *27*, 43–50.
(25) (a) Atilgan, S.; Ekmekci, Z.; Dogan, A. L.; Guc, D.; Akkaya, E. U. *Chem. Commun.* **2006**, 4398–4400. (b) Ramaiah, D.; Eckert, I.; Arun, K. T.; Weidenfeller, L.; Epe, B. *Photochem. Photobiol.* **2004**, *79*, 99–104. (c) Kar, M.; Basak, A. *Chem. Rev.* **2007**, *107*, 2861–2890.
(26) Szacilowski, K.; Macyk, W.; Drzewiecka-Matuszek, A.; Brindell, M.; Stochel, G. *Chem. Rev.* **2005**, *105*, 2647–2694.
(27) Burrows, C. J.; Muller, J. G. *Chem. Rev.* **1998**, *98*, 1109–1152.
(28) (a) Farrer, N. J.; Salassa, L.; Sadler, P. J. *Dalton Trans.* **2009**, 10690–10701. (b) Mackay, F. S.; Woods, J. A.; Heringová, P.; Kašpárková, J.; Pizarro, A. M.; Moggach, S. A.; Parsons, S.; Brabec, V.; Sadler, P. J. *Proc. Natl. Acad. Sci. U. S. A.* **2007**, *104*, 20743–48. (c) Benites, P. J.; Holmberg, R. C.; Rawat, D. S.; Kraft, B. J.; Klein, L. J.; Peters, D. G.; Thorp, H. H.; Zaleski, J. M. *J. Am. Chem. Soc.* **2003**, *125*, 6434–6446. (d) Maisch, T. *Lasers Med. Sci.* **2007**, *22*, 83–91.
(29) (a) Ostrowski, A. D.; Ford, P. C. *Dalton Trans.* **2009**, 10660–10669. (b) Rose, M. J.; Fry, N. L.; Marlow, R.; Hinck, L.; Mascharak, P. K. *J. Am. Chem. Soc.* **2008**, *130*, 8834–8846.
(30) (a) Chifotides, H. T.; Dunbar, K. R. *Acc. Chem. Res.* **2005**, *38*, 146–156. (b) Angeles-Boza, A. M.; Chifotides, H. T.; Aguirre, J. D.; Chouai, A.; Fu, P. K.-L.; Dunbar, K. R.; Turro, C. *J. Med. Chem.* **2006**, *49*, 6841–6847.
(31) Saha, S.; Majumdar, R.; Roy, M.; Dighe, R. R.; Chakravarty, A. R. *Inorg. Chem.* **2009**, *48*, 2652–2663.
(32) Sasmal, P. K.; Saha, S.; Majumdar, R.; Dighe, R. R.; Chakravarty, A. R. *Chem. Commun.* **2009**, 1703–1705.
(33) Hurley, A. L.; Mohler, D. L. *Org. Lett.* **2000**, *2*, 2745–2748.
(34) (a) Herebian, D.; Sheldrick, W. S. *J. Chem. Soc., Dalton Trans.* **2002**, 966–974. (b) Schoch, T. K.; Hubbard, J. L.; Zoch, C. R.; Yi, G.-B.; Sørlie, M. *Inorg. Chem.* **1996**, *35*, 4383–4390.
(35) Niesel, J.; Pinto, A.; N'Dongo, H. W. P.; Merz, K.; Ott, I.; Gust, R.; Schatzschneider, U. *Chem. Commun.* **2008**, 1798–1800.
(36) (a) Riordan, C. G.; Wei, P. *J. Am. Chem. Soc.* **1994**, *116*, 2189–2190. (b) Magennis, S. W.; Habtemariam, A.; Novakova, O.; Henry, J. B.; Meier, S.; Parsons, S.; Oswald, I. D. H.; Brabec, V.; Sadler, P. J. *Inorg. Chem.* **2007**, *46*, 5059–5068. (c) Betanzos-Lara, S.; Salassa, L.; Habtemariam, A.; Sadler, P. J. *Chem. Commun.* **2009**, 6622–6624.
(37) Mohler, D. L.; Downs, J. R.; Hurley-Predecki, A. L.; Sallman, J. R.; Gannett, P. M.; Shi, X. *J. Org. Chem.* **2005**, *70*, 9093–9102.
(38) Shimakoshi, H.; Kaieda, T.; Matsuo, T.; Sato, H.; Hisaeda, Y. *Tetrahedron Lett.* **2003**, *44*, 5197–5199.
(39) (a) Maity, B.; Roy, M.; Saha, S.; Chakravarty, A. R. *Organometallics* **2009**, *28*, 1495–1505. (b) Maity, B.; Roy, M.; Chakravarty, A. R. *J. Organomet. Chem.* **2008**, *693*, 1395–1399.
(40) Goswami, T. K.; Roy, M.; Nethaji, M.; Chakravarty, A. R. *Organometallics* **2009**, *28*, 1992–1994.

Table 1. Selected Physicochemical Data and DNA Binding Parameters for Complexes 1−4

complex	IR[a]/cm^{-1} [ν(ClO_4^-)]	λ_{max}/nm (ε /M^{-1} cm^{-1})[b]	E_f/V (ΔE_p/mV)[c]	μ_{eff}[d]/μ_B	K_b[e]/M^{-1} [s]	ΔT_m[f]/°C
[Cu(Fc-tpy)(phen)](ClO_4)$_2$ (**1**)	1095	410 (1720), 545 (3225)	0.45 (110)[g] −0.29 (145)[h]	1.81	1.4 (±0.8) × 10^4 [0.05]	7.6
[Cu(Fc-tpy)(dpq)](ClO_4)$_2$ (**2**)	1088	411 (1710), 546 (3030)	0.47 (120)[g] −0.23 (140)[h]	1.79	2.4 (±0.5) × 10^5 [0.08]	8.1
[Cu(Fc-tpy)(dppz)](ClO_4)$_2$ (**3**)	1090	413 (2060), 546 (3760)	0.44 (90)[g] −0.34 (105)[h]	1.77	4.3 (±0.4) × 10^5 [0.12]	9.2
[Cu(Ph-tpy)(dppz)](ClO_4)$_2$ (**4**)	1094	433 (215), 640 (80)	−0.30 (120)[h]	1.80	5.6 (±0.6) × 10^5 [0.11]	9.7

[a] In KBr phase. [b] In 15% aqueous DMF. The d−d band for **1**−**3** could not be observed due to the presence of an intense band at ∼545 nm. [c] Redox couple(s) in 30% aqueous DMF−0.1 M KCl, $E_f = 0.5(E_{pa} + E_{pc})$, $\Delta E_p = (E_{pa} - E_{pc})$, where E_{pa} and E_{pc} are the anodic and cathodic peak potentials, respectively. The potentials are vs SCE. Scan rate = 50 mV s^{-1}. The ligand reduction data are −1.6 V for **1**, −1.2 and −1.6 V for **2**, −1.0 and −1.6 V for **3**, and −1.2 and −1.7 V for **4**. [d] Magnetic moment at 298 K using solid powdered samples of the complexes. [e] Intrinsic equilibrium DNA binding constant and binding site size value are from UV−visible experiment. [f] Change in CT DNA melting temperature. [g] The Fc^+−Fc redox couple [Fc = (η^5-C_5H_4)Fe^{II}(η^5-C_5H_5)]. [h] The Cu(II)−Cu(I) redox couple.

Chart 1. Schematic Drawing of the Complexes [Cu(Fc-tpy)(B)](ClO_4)$_2$ (B = phen in 1; dpq in 2; dppz in 3) and [Cu(Ph-tpy)(dppz)](ClO_4)$_2$ (4)

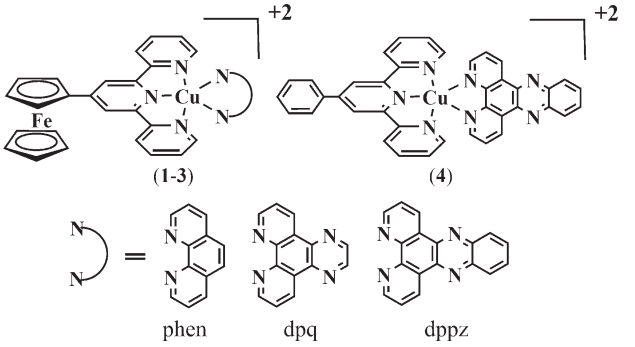

(∼60−80%) from the reaction of copper(II) nitrate, ferrocenyl terpyridine ligand (Fc-tpy), and the respective phenanthroline base (B) in a chloroform−methanol mixture (B: phen, **1**; dpq, **2**; dppz, **3**). The complexes were isolated as perchlorate salts. Complex [Cu(Ph-tpy)(dppz)](ClO_4)$_2$ (**4**) was prepared to study the role of the ferrocenyl moiety in **1**−**3** toward DNA binding and cleavage activity. The complexes were characterized from spectral and analytical data (Table 1). The complexes showed structural stability in the solution phase, as evidenced from the mass spectra displaying a prominent molecular ion peak (m/z) that corresponds to the $[M - 2ClO_4]^{2+}$ species (Figures S1−S4, Supporting Information). Molar conductivity measurements at 25 °C in DMF gave values of 135−150 S m^2 M^{-1}, indicating the 1:2 electrolytic nature of the complexes. The presence of perchlorate anion in the complexes was evidenced from the IR spectra showing a characteristic ClO_4^- frequency near 1090 cm^{-1} (Figures S5−S8, Supporting Information). The electronic spectra of the complexes were recorded in aqueous DMF (15% DMF). Complexes **1**−**3** show a ferrocene-centered band at ∼410 nm with an additional charge transfer band at ∼545 nm, which is absent in free Fc-tpy ligand (L) (Figure 1, Figure S9, Supporting Information).[41] A similar charge transfer band near 520−540 nm is reported for the Fe(II), Zn(II), and Ru(II) complexes of the ferrocenyl terpyridyl ligand.[42] The low-intensity copper-centered d−d band is not observed, possibly due to masking by this high-intensity charge transfer band.

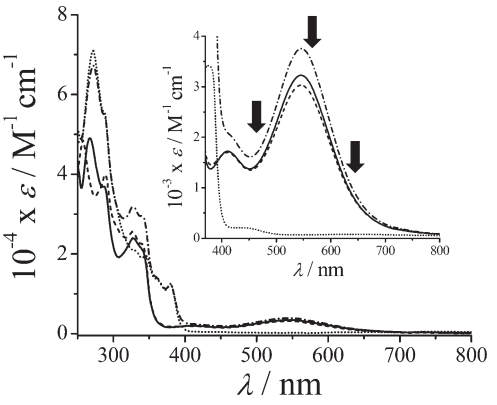

Figure 1. Electronic absorption spectra of [Cu(Fc-tpy)(B)](ClO_4)$_2$ (B = phen in **1** (—); dpq in **2** (---); dppz in **3** (-·-·-)) and [Cu(Ph-tpy)(dppz)](ClO_4)$_2$ (**4**) (···) in Tris−HCl buffer containing 15% DMF. The arrows indicate the wavelengths of laser light used for photoinduced DNA cleavage studies.

Complex **4**, which lacks the ferrocenyl moiety, however, shows a low-energy copper(II)-centered d−d band at 640 nm (Figure 1). The complexes also show ligand-centered bands in the UV region. The band at ∼288 nm could be due to the terpyridyl moiety. The dppz complexes **3** and **4** show an n→π^* transition at ∼360 and 380 nm, respectively, while this transition for the dpq complex is observed at ∼340 nm.[43] The solution stability of the complexes in aqueous medium was also evidenced from the UV−visible spectral study. The spectral features did not change on keeping the solutions for 6 h in aqueous DMF (1:1 v/v) in the dark, indicating structural stability of the complexes (Figure S10, Supporting Information). Cyclic voltammetric experiments for the complexes were carried out in 30% DMF−water using 0.1 M KCl as the supporting electrolyte. All the complexes are redox active and show a quasi-reversible voltammetric response near −0.3 V vs SCE due to the Cu(II)−Cu(I) redox couple (Figure 2, Figure S11, Supporting Information). The ferrocenyl moiety in **1**−**3** is redox active, showing a nearly reversible voltammogram at ∼0.45 V. The complexes showed ligand reductions within −1.2 and −1.7 V vs SCE (Table 1).

Crystal Structures. Complexes **1** and **3** as their PF_6^- salts (**1a**, **3a**) were structurally characterized by single-crystal X-ray diffraction. Complex **1a** crystallized in the $C2/c$ space group of the monoclinic crystal system, while the crystals of

(41) Farlow, B.; Nile, T. A.; Wals, J. L. *Polyhedron* **1993**, *12*, 2891–2894.

(42) Hutchison, K.; Morris, J. C.; Nile, T. A.; Walsh, J. L.; Thompson, D. W.; Petersen, J. D.; Schoonover, J. R. *Inorg. Chem.* **1999**, *38*, 2516–2523.

(43) Toshima, K.; Takano, R.; Ozawa, T.; Matsumura, S. *Chem. Commun.* **2002**, 212–213.

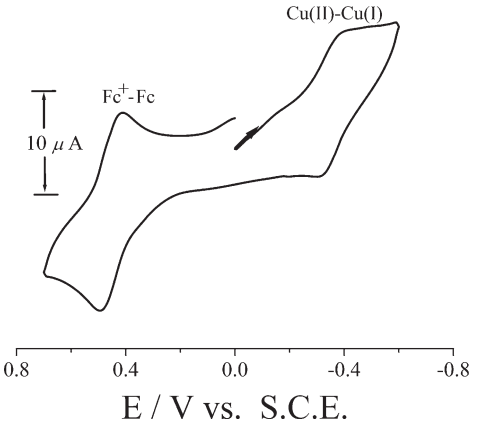

Figure 2. Cyclic voltammogram showing the Fc^+-Fc and Cu(II)−Cu(I) redox couples in $[Cu(Fc\text{-}tpy)(dppz)](ClO_4)_2$ (**3**) in 30% aqueous DMF−0.1 M KCl at a scan rate of 50 mV s^{-1} [Fc = $(\eta^5\text{-}C_5H_4)Fe^{II}(\eta^5\text{-}C_5H_5)$].

Table 2. Selected Bond Distances (Å) and Bond Angles (deg) for [Cu(Fc-tpy)(phen)]$(PF_6)_2$ (1a) and [Cu(Fc-tpy)(dppz)]-$(PF_6)_2\cdot CH_3CN$ (3a)

	1a	3a
Cu(1)−N(1)	2.045(5)	2.046(3)
Cu(1)−N(2)	1.906(4)	1.924(2)
Cu(1)−N(3)	2.034(4)	2.051(3)
Cu(1)−N(4)	1.980(4)	2.015(2)
Cu(1)−N(5)	2.249(5)	2.188(2)
Fe(1)−C_0^1 [Fe(1)−C_0^2][a]	1.638 [1.630]	1.645 [1.634]
N(1)−Cu(1)−N(2)	79.76(19)	79.33(10)
N(1)−Cu(1)−N(3)	157.22(18)	157.58(10)
N(1)−Cu(1)−N(4)	98.14(19)	100.90(10)
N(1)−Cu(1)−N(5)	95.09(17)	94.95(9)
N(2)−Cu(1)−N(3)	80.44(18)	80.24(10)
N(2)−Cu(1)−N(4)	176.72(19)	173.05(9)
N(2)−Cu(1)−N(5)	103.47(18)	107.64(9)
N(3)−Cu(1)−N(4)	101.10(18)	98.28(10)
N(3)−Cu(1)−N(5)	100.39(17)	99.95(10)
N(4)−Cu(1)−N(5)	79.17(17)	79.29(9)

[a] C_0^1 and C_0^2 are two centroids of the cyclopentadienyl rings comprising atoms C(1) to C(5) and C(6) to C(10) for **1a** and C(39) to C(43) and C(34) to C(38) for **3a**, respectively. The Fe(1)−C distances are in the range 1.995(11) to 2.038(7) Å for **1a**, giving an average value of 2.018 Å. The Fe(1)−C distances are in the range 2.007(4) to 2.049(4) Å for **3a**, giving an average value of 2.032 Å.

complex **3a** belonged to the $P\bar{1}$ space group of the triclinic system. The molecular structures of both **1a** and **3a** showed a distorted square-pyramidal geometry around the copper(II) center with the Fc-tpy and the phenanthroline base showing a tridentate and bidentate mode of binding, respectively. The Fc-tpy binds at the basal plane, and the phenanthroline base shows an axial−equatorial binding mode. Selected bonding parameters are given in Table 2. The perspective views of the molecules are shown in Figures 3 and 4 (Figures S12, S13, Supporting Information). The Cu−N distances in the basal plane are ∼2.0 Å, while the axial Cu−N distances are ∼2.2 Å. The Cu−N bond distance involving the central pyridyl ring of Fc-tpy is shorter than the other Cu−N bond distances involving the terminal pyridyl groups. The structural distortion parameter (τ) values for **1a** and **3a** are 0.32 and 0.25, respectively, indicating significant distortion in the square-pyramidal geometry.[44] Two cyclopentadienyl rings of the

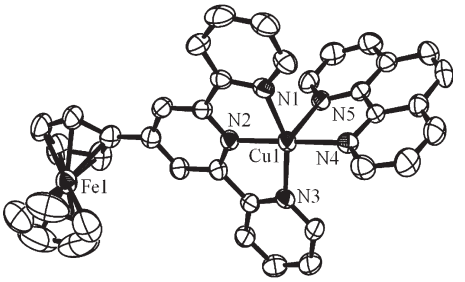

Figure 3. ORTEP view of the cationic complex of [Cu(Fc-tpy)(phen)]$(PF_6)_2$ (**1a**) showing 50% probability thermal ellipsoids and the atom-numbering scheme for the metal and heteroatoms. The hydrogen atoms are not shown for clarity.

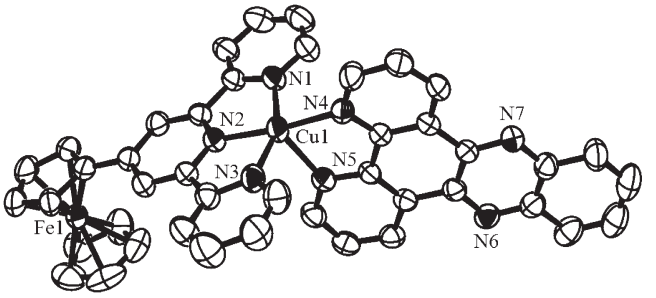

Figure 4. ORTEP view of the cationic complex in [Cu(Fc-tpy)-(dppz)]$(PF_6)_2\cdot CH_3CN$ (**3a**) showing 50% probability thermal ellipsoids and the atom-numbering scheme for the metal and heteroatoms. The hydrogen atoms are omitted for clarity.

ferrocenyl moiety in both the complexes are essentially in eclipsed conformation. A significant $\pi-\pi$ stacking interaction was observed in the **1a** structure involving two planar phenanthroline rings belonging to two different molecules within the unit cell (Figure S14, Supporting Information). The interplanar distance between two phenanthroline rings is ∼3.484 Å. The two axial F atoms of one of the PF_6 anions show a significant intermolecular short contact interaction (∼2.751 Å) with two copper atoms (Figure S15, Supporting Information). In **3a**, the terpyridyl moiety and the cyclopentadienyl ring of ferrocene are found to be involved in intermolecular $\pi\cdots\pi$ stacking interactions, giving an interplanar distance of ∼3.334 Å (Figure S16, Supporting Information).

DNA Binding Properties. DNA binding propensity of the complexes to calf thymus (CT) DNA was studied by using various experimental techniques. Selected DNA binding data are presented in Table 1. Equilibrium binding constant (K_b) and the binding site size (s) values of the complexes to CT-DNA were determined from UV−visible absorption titration experiments (Figure 5, Figure S17, Supporting Information). Addition of CT-DNA to a 20 μM complex concentration in Tris−HCl buffer medium (pH 7.2) showed a significant hypochromicity (∼10−20%) at ∼270 nm with a minor bathochromic shift of ∼2 nm. The K_b values of **1**−**4** are in the range $1.4(\pm0.8)\times10^4$ to $5.6(\pm0.6)\times10^5$ M^{-1}. The complexes are avid binders to CT-DNA, and the binding site size values ($s \le 1$) are indicative of the groove-binding nature of the complexes.[45] The stability of the duplex DNA on complex binding was studied by the thermal denaturation

(44) Addison, A. W.; Rao, T. N.; Reedijk, J. V.; Verschoor, G. C. *J. Chem. Soc., Dalton Trans.* **1984**, 1349–1356.

(45) Angeles-Boza, A. M.; Bradley, P. M.; Fu, P. K.-L.; Wicke, S. E.; Bacsa, J.; Dunbar, K. R.; Turro, C. *Inorg. Chem.* **2004**, *43*, 8510–8519.

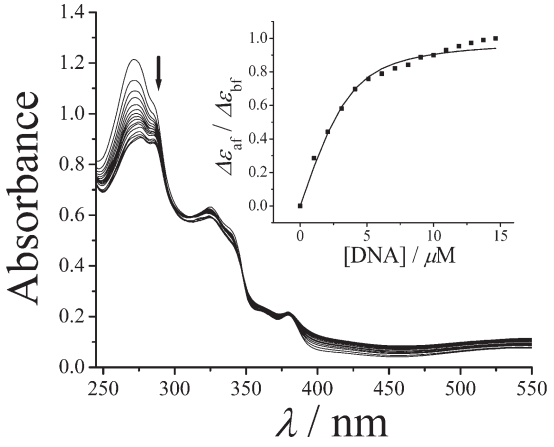

Figure 5. Spectral traces showing the effect of gradual addition of CT-DNA (210 μM NP) to the 20 μM solution of [Cu(Fc-tpy)(dppz)]$(ClO_4)_2$ (**3**) in DMF−Tris−HCl buffer medium. The inset shows the plot of $\Delta\varepsilon_{af}/\Delta\varepsilon_{bf}$ vs. [DNA].

method. The DNA duplex is known to cooperatively unwind at melting temperature (T_m) to give single-stranded DNA with a significant increase in the absorbance value at 260 nm.[46] The complexes showed a large increase in the DNA melting temperature of ~7−10 °C, indicating significant stabilization of the double helical structure of calf thymus DNA on binding to the complexes (Figure 6). Similar ΔT_m values are known for the terpyridyl ruthenium complexes having phenanthroline bases.[47] The relative DNA binding affinity of the complexes based on the ΔT_m values follows the order {(Ph-tpy)Cu(dppz)} (**4**) ≥ {(Fc-tpy)Cu(dppz)} (**3**) > {(Fc-tpy)Cu-(dpq)} (**2**) > {(Fc-tpy)Cu(phen)} (**1**). The ΔT_m values of ~9.0 °C, observed for the dipyridophenazine complexes **3** and **4**, are lower than the ΔT_m value of 14.0 °C measured for the classical DNA intercalator ethidium bromide under similar experimental conditions. The DNA binding nature of the complexes was also studied by the viscometric titration method. An intercalative mode of binding of the complex to DNA is expected to result in significant lengthening of the DNA helix as the base pairs get separated to accommodate the intercalator, thus leading to an increase in DNA relative specific viscosity.[48] In contrast, a partial intercalation and/or groove binding is likely to cause a minor or no change in the relative viscosity of the DNA solution. The effect of increasing concentration of the complexes on the relative specific viscosity $(\eta/\eta_0)^{1/3}$ (where η and η_0 are the specific viscosity of DNA in the presence and absence of the complex, respectively) of the DNA solution is shown in Figure 6. The plots suggest primarily groove binding propensity of the phen and dpq complexes, while the dppz complexes show a partial intercalative mode of DNA binding. Ethidium bromide displays a significant increase in the relative specific viscosity, while DNA minor groove binder Hoechst 33258 dye shows only a minor increase in relative viscosity. The DNA binding data do not show any apparent steric effect of the ferrocenyl moiety when compared to that of the control species.

Chemical Nuclease Activity. The chemical nuclease activity of the complexes **1**−**4** was studied in air by agarose gel electrophoresis in the presence of 3-mercaptopropionic acid (MPA) as a reducing agent and H_2O_2 as an oxidizing species using supercoiled (SC) pUC19 DNA (0.2 μg, 30 μM) (Figure 7). A 10 μM concentration of the dppz complexes **3** and **4** showed essentially complete cleavage of SC DNA into its nicked circular (NC) form in the presence of MPA or H_2O_2. The dpq complex **2** also displayed significant chemical nuclease activity, giving ~75% NC DNA form under similar experimental conditions. The phen complex **1** showed only moderate chemical nuclease activity (~55% NC form). The external agents MPA and H_2O_2 or the phenanthroline bases alone did not show any apparent chemical nuclease activity. Fc-tpy showed ~25% cleavage activity in the presence of H_2O_2. The chemical nuclease activity of the complexes follows their DNA binding order: **4** ~ **3** > **2** > **1**. The mechanistic aspects of the chemical nuclease activity were studied using different additives and complex **3** (Figure S18, Supporting Information). Singlet oxygen quenchers, namely, NaN_3, TEMP, and DABCO did not show any apparent effect on the chemical nuclease activity of the complexes in the presence of MPA or H_2O_2. Hydroxyl radical scavengers, namely, DMSO, mannitol, and KI, showed significant inhibition in the DNA cleavage activity, indicating the involvement of diffusible hydroxyl radicals for the chemical nuclease activity of the complexes. The inhibition in the presence of catalase indicates the formation of O_2^{2-} as an intermediate species prior to the generation of hydroxyl radicals. The reaction in the presence of MPA could form reduced Cu(I) species that can activate molecular oxygen to generate $^{\bullet}OH$ radical following a mechanistic pathway that is known for the chemical nuclease activity of bis-phen copper species.[49] The reaction in the presence of H_2O_2 could involve formation of reactive ferrocenium species that can generate hydroxyl radicals via a Fenton-type reaction. The groove binding propensity of the complexes was determined in the presence of DNA major groove binder methyl green (500 μM) and minor groove binder distamycin-A (500 μM). Complexes **3** and **4** displayed significant reduction in the chemical nuclease activity in the presence of methyl green, while similar inhibition for the complexes **1** and **2** was observed in the presence of distamycin-A. The results indicate minor groove binding propensity for the phen and dpq complexes (**1**, **2**) and major groove binding preference for the dppz complexes **3** and **4** (Figure S19, Supporting Information).

Photoactivated DNA Cleavage. The photoinduced DNA cleavage activity of the complexes in visible light of 458, 568, and 647 nm wavelengths was studied by gel electrophoresis using supercoiled pUC19 DNA in 50 mM Tris−HCl/NaCl buffer (pH 7.2) under aerobic condition (Figure 8). The choice of these wavelengths was based on the visible spectral bands observed for the complexes. Selected DNA photocleavage data are given in Table 3. The dppz complexes showed efficient photocleavage of DNA in red light of 647 nm. The observed order is {(Fc-tpy)Cu(dppz)} (**3**) > {(Fc-tpy)Cu(dpq)} (**2**) ≥ {(Ph-tpy)Cu-(dppz)} (**4**) > {(Fc-tpy)Cu(phen)} (**1**). The photoactivated dppz complex **3**, having a ferrocene-apppended terpyridyl ligand, exhibits better DNA cleavage activity than its Ph-tpy analogue **4**, indicating the positive role of the ferrocenyl moiety in the DNA cleavage reaction. The free ligands and metal salt

(46) Kelly, J. M.; Tossi, A. B.; McConnell, D. J.; OhUigin, C. *Nucl. Acid Res.* **1985**, *13*, 6017–6034.
(47) Neyhart, G. A.; Grover, N.; Smith, S. R.; Kalsbeck, W. A.; Fairley, T. A.; Cory, M.; Thorp, H. H. *J. Am. Chem. Soc.* **1993**, *115*, 4423–4428.
(48) Veal, J. M.; Rill, R. L. *Biochemistry* **1991**, *30*, 1132–1140.
(49) (a) Thederahn, T. B.; Kuwabara, M. D.; Larsen, T. A.; Sigman, D. S. *J. Am. Chem. Soc.* **1989**, *111*, 4941–4946. (b) Zelenko, O.; Gallagher, J.; Sigman, D. S. *Angew. Chem., Int. Ed. Engl.* **1997**, *36*, 2776–2778. (c) Sigman, D. S.; Mazumder, A.; Perrin, D. M. *Chem. Rev.* **1993**, *93*, 2295–2316. (d) Sigman, D. S.; Bruice, T. W.; Mazumder, A.; Sutton, C. L. *Acc. Chem. Res.* **1993**, *26*, 98–104. (e) Marshall, L. E.; Graham, D. R.; Reich, K. A.; Sigman, D. S. *Biochemistry* **1981**, *20*, 244–250.

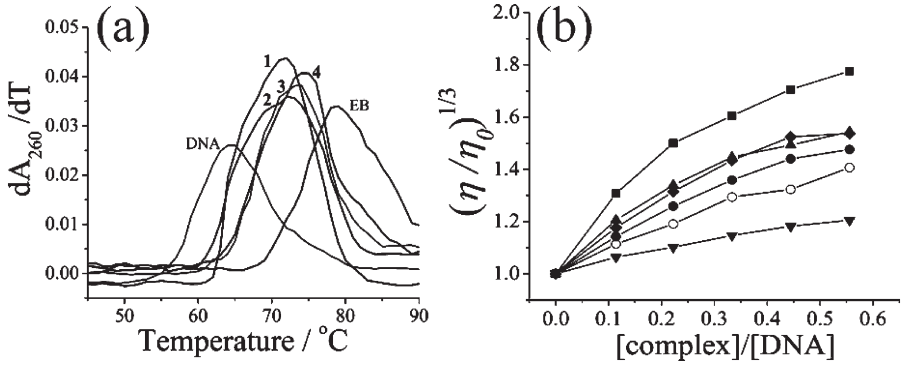

Figure 6. (a) DNA melting plots for the CT-DNA (160 μM NP) alone and in the presence of complexes **1**−**4** (20 μM) and ethidium bromide (EB, 20 μM) in 5 mM phosphate buffer (pH = 6.8). (b) Effect of addition of increasing amounts of the complexes **1** (○), **2** (●), **3** (♦), and **4** (▲) along with the DNA intercalator EB (■) and DNA minor groove binder Hoechst 33258 (▼) on the relative viscosity of CT-DNA at 37.0(±0.1) °C in 5 mM Tris−HCl buffer (pH = 7.2).

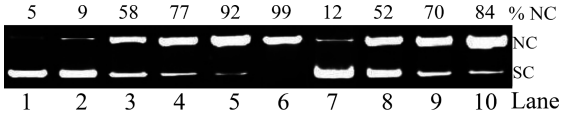

Figure 7. Gel electrophoresis diagram showing the chemical nuclease activity of the complexes [Cu(Fc-tpy)(B)]$(ClO_4)_2$ (B = phen in **1**; dpq in **2**; dppz in **3**) and [Cu(Ph-tpy)(dppz)]$(ClO_4)_2$ (**4**) (10 μM) using SC pUC19 DNA (0.2 μg, 30 μM b.p.) in the presence of 0.5 mM 3-mercaptopropionic acid (MPA) as a reducing and 0.25 mM H_2O_2 as an oxidizing agent: lane 1, DNA control; lane 2, DNA + MPA; lane 3, DNA + **1** + MPA; lane 4, DNA + **2** + MPA; lane 5, DNA + **3** + MPA; lane 6, DNA + **4** + MPA; lane 7, DNA + H_2O_2; lane 8, DNA + **1** + H_2O_2; lane 9, DNA + **2** + H_2O_2; lane 10, DNA + **3** + H_2O_2.

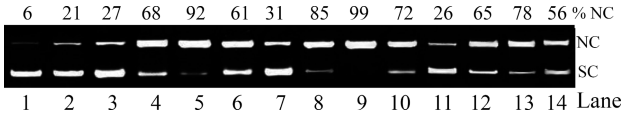

Figure 8. Gel electrophoresis diagram showing the visible light-induced DNA cleavage activity of the complexes [Cu(Fc-tpy)(B)]$(ClO_4)_2$ (B = phen in **1**; dpq in **2**; dppz in **3**) and [Cu(Ph-tpy)(dppz)]$(ClO_4)_2$ (**4**) (15 μM) using SC pUC19 DNA (0.2 μg, 30 μM b.p.) for a photoexposure time of 2 h: lane 1, DNA control (458 nm); lane 2, DNA + Fc-tpy (15 μM) (458 nm); lane 3, DNA + **1** (458 nm); lane 4, DNA + **2** (458 nm); lane 5, DNA + **3** (458 nm); lane 6, DNA + **4** (458 nm); lane 7, DNA + **1** (568 nm); lane 8, DNA + **2** (568 nm); lane 9, DNA + **3** (568 nm); lane 10, DNA + **4** (568 nm); lane 11, DNA + **1** (647 nm); lane 12, DNA + **2** (647 nm); lane 13, DNA + **3** (647 nm); lane 14, DNA + **4** (647 nm).

did not show any significant DNA photocleavage activity under similar conditions (Figure S20, Supporting Information). The complexes did not show any apparent DNA cleavage in the dark, thus eliminating the possibility of hydrolytic cleavage of DNA involving the phosphodiester bond.

The mechanistic aspects of the DNA photocleavage reactions of **3** were studied using different additives as hydroxyl radical scavengers (e.g., dimethyl sulfoxide (DMSO), catalase, and potassium iodide (KI)) and singlet oxygen quenchers (e.g., sodium azide and 2,2,6,6-tetramethyl-4-piperidone (TEMP)) in visible light of 458 and 568 nm (Figure 9). Significant inhibition in DNA cleavage was observed in the presence of hydroxyl radical scavengers. The singlet oxygen quenchers did not show any inhibition in the DNA photocleavage reaction. The results

Table 3. Selected SC pUC19 DNA (0.2 μg, 30 μM b.p.) Cleavage Data for the Complexes [Cu(Fc-tpy)(B)]$(ClO_4)_2$ (B = phen in 1; dpq in 2; dppz in 3) and [Cu(Ph-tpy)(B)]$(ClO_4)_2$ (4)

Sl. no.	reaction condition	λ^a/nm ([complex]/μM)	% NC[b]
1	DNA control	458	6
2	DNA + **1**	458 (15)	27
		568 (15)	31
		647(15)	26
3	DNA + **2**	458 (15)	68
		568 (15)	85
		647(15)	65
4	DNA + **3**	458 (15)	92
		568 (15)	99
		647(15)	78
5	DNA + **4**	458 (15)	61
		568 (15)	72
		647 (15)	56

[a] Wavelength used for DNA cleavage in air, λ = 458, 568, and 647 nm (50 mW). Exposure time (t) = 2 h. [b] NC is the nicked circular form of DNA obtained from the cleavage of SC DNA.

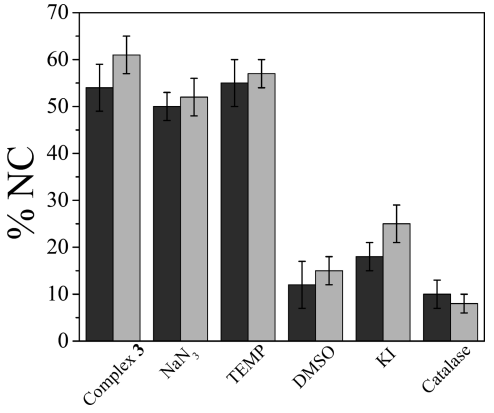

Figure 9. Bar diagram showing the photoinduced pUC19 DNA (0.2 μg, 30 μM b.p.) cleavage activity of [Cu(Fc-tpy)(dppz)]$(ClO_4)_2$ (**3**) (15 μM) in the presence of different singlet oxygen quenchers and hydroxyl radical scavengers using laser wavelengths of 458 nm (dark shade) and 568 nm (light shade) for an exposure time of 1 h [concentrations of the additives: NaN_3, TEMP, KI of 0.5 mM; DMSO = 6 μL; catalase = 8 units].

indicate the formation of hydroxyl radicals as the cleavage-active species. The formation of hydroxyl radical could take place via a photoredox pathway involving the redox-active

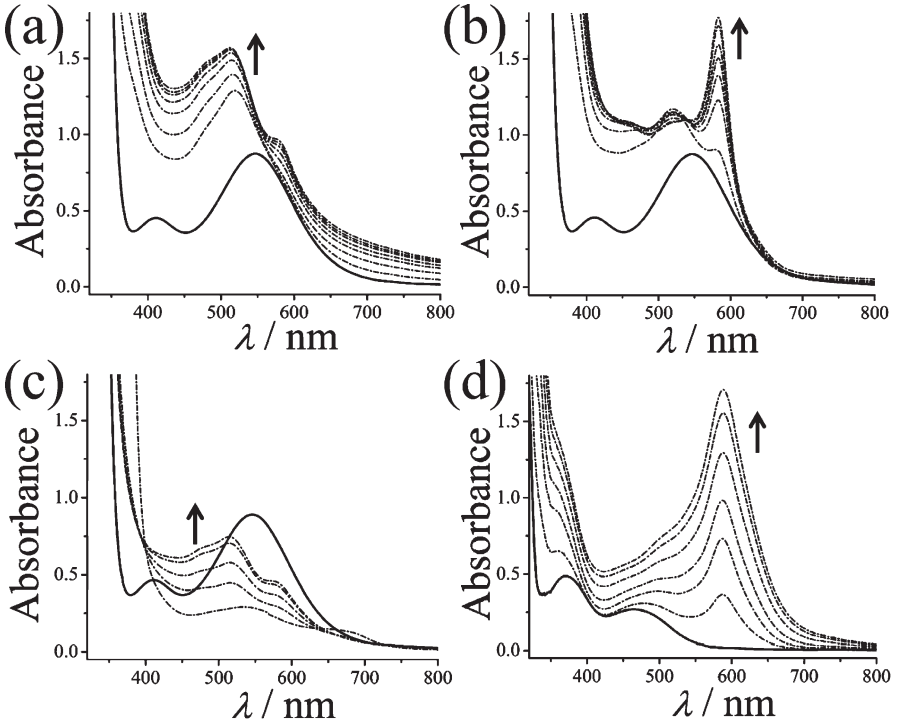

Figure 10. Absorption spectral changes of the phen complex **1** or Fc-tpy (250 μM) in aqueous DMF under different reaction conditions: (a) photoirradiation of the phen complex **1** in air in UV-A light of 365 nm, (b) photoirradiation of complex **1** under argon in UV-A light of 365 nm and spectral traces at 3 min intervals, (c) complex **1** on treatment with ceric(IV) ammonium nitrate (30 mM stock solution in water) in air, and (d) Fc-tpy on exposure to UV-A light of 365 nm in air and spectral traces at 3 min intervals. The solid lines indicate the initial spectra at $t = 0$ min.

metal centers.[27] We did UV photolysis experiments using the phen complex **1**. The complex shows visible bands at 410 and 545 nm in Tris−HCl buffer medium containing 25% DMF. Photoirradiation of complex **1** in air using UV-A light of 365 nm showed the appearance of three new visible bands, at ~580, ~510, and ~480 nm (Figure 10). There was, however, no apparent change in the visible spectra for a sample that was left unexposed to light. The electronic spectrum of complex **4** in the absence of the ferrocenyl moiety did not show any apparent spectral change upon photoirradiation in UV-A light (Figure S21, Supporting Information). Again, addition of an oxidizing agent such as ceric(IV) ammonium nitrate to the Fc-tpy ligand alone in aqueous DMF (1:1) gave an intense charge transfer band at ~585 nm, and this band could be assigned to the oxidized ferrocenyl moiety (Figure S21, Supporting Information). A similar observation was made when Fc-tpy ligand was irradiated in air with UV-A light of 365 nm in the absence of $(NH_4)_2[Ce(NO_3)_6]$ (Figure 10). Therefore, the absorption band at ~580 nm, observed for **1** on photoirradiation, could be due to the formation of ferrocenium ion in an aqueous-DMF medium. The oxidized ferrocenyl moiety in **1** could readily degrade in aqueous-DMF to form the Fe(II)-phen complex as well as ferrocene.[18,50] The electronic absorption bands at ~510 and ~480 nm, observed after photoirradiation of complex **1**, could be due to MLCT bands of the Fe(II)-phen species.[51] Photo-oxidation of the ferrocenyl moiety was further evidenced from the appearance of the visible bands at ~480 and ~510 nm along with a band at 585 nm upon photoirradiation of a mixture of Fc-tpy ligand and free phenanthroline base at 365 nm. A similar experiment in the presence of phenanthrene that lacks any metal binding site gave only a band at 585 nm under similar reaction conditions (Figure S21, Supporting Information). Complex **1**, upon addition of ceric(IV) ammonium nitrate, also resulted in similar visible bands (Figure 10). The results indicate that the ferrocenyl moiety in the complexes plays an important role in generating cleavage-active hydroxyl radicals. Further, the presence of the {(terpyridyl)-Cu(II)} moiety in these complexes could facilitate the charge transfer process on photoactivation due to formation of the reduced Cu(I) species, which could activate molecular oxygen to generate hydroxyl radicals.[49] Under anaerobic conditions, photoirradiation of complex **1** showed predominantly the 580 nm absorption band, indicating the essential requirement of molecular oxygen to degrade the oxidized ferrocenyl moiety (Figure 10). Similar spectral results were obtained for complex **3** (Figure S21, Supporting Information). The generation of reactive hydroxyl radicals could thus proceed via a photoredox pathway involving both the Cu(II) and the ferrocenyl moiety.

Cytotoxicity in HeLa Cells. The anticancer activity of the dppz complexes **3** and **4** toward HeLa cells was examined by MTT assay. Both the complexes showed significant cytotoxicity, giving respective IC_{50} values of 10.5 and 13.7 μM, whereas the free ligand dppz (IC_{50} = 52 μM in light and > 100 μM in dark) and Ph-tpy (IC_{50} > 100 μM in both dark and light) did not show any significant cytotoxicity (Figure S22 Supporting Information). The cytotoxicity of the Fc-tpy ligand could not be measured due to its insolubility in the buffer medium. A 2-fold increase in photocytotoxicity was

(50) (a) Hurvois, J. P.; Moinet, C. *J. Organomet. Chem.* **2005**, *690*, 1829–1839. (b) Prins, R.; Korswagen, A. R.; Kortbeek, A. G. T. G. *J. Organomet. Chem.* **1972**, *39*, 335–344. (c) Yamaguchi, Y.; Ding, W.; Sanderson, C. T.; Borden, M. L.; Morgan, M. J.; Kutal, C. *Coord. Chem. Rev.* **2007**, *251*, 515–524.

(51) Mudasir; Yoshioka, N.; Inoue, H. *Transition Met. Chem.* **1999**, *24*, 210–217.

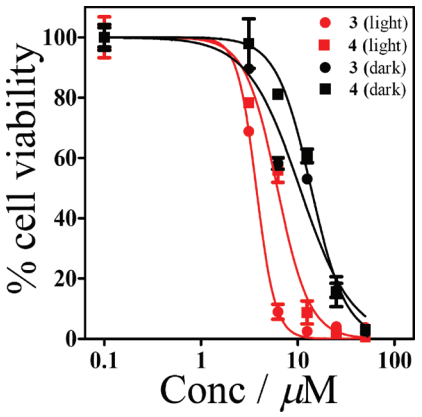

Figure 11. Cytotoxicity of complexes **3** and **4** in human cervical HeLa cancer cells on 3 h incubation in the dark followed by photoirradiation to visible light (400 to 700 nm) as determined by the MTT assay. The dark-treated and photoexposed cells are shown by black and red symbols, respectively.

observed in visible light of wavelength 400−700 nm, and the photoactivated IC_{50} values for **3** and **4** were 3.7 and 6.1 μM (Figure 11). The ferrocenyl moiety in **3** is found to enhance the cytotoxicity of the complex in comparison to its analogue having a phenyl group. The photocytoxicity of complex **3** is similar to that of Photofrin, for which the IC_{50} values are 4.3 μM in red light and >41 μM in the dark.[52] The IC_{50} value of **3** in visible light is also comparable to those known for the iron(III) and oxovanadium(IV) complexes having a dppz ligand.[31,32] Cisplatin does not show any photocytotoxic effect in HeLa cells, and the IC_{50} value of cisplatin is significantly higher than that of Photofrin in red light.[53]

Conclusions

A new series of ferrocene-appended terpyridine copper(II) complexes having phenanthroline bases are prepared and structurally characterized, and their DNA binding and photoinduced DNA cleavage activity in visible light and cytotoxicity in HeLa cells were studied. We have prepared the copper(II) complex of the Ph-tpy ligand as a control species to explore the role of the ferrocenyl moiety in the DNA cleavage reactions. All the complexes are avid binders to DNA. The complexes having a dipyridophenazine ligand show a partial intercalative mode of DNA binding. The complexes are redox active and show quasi-reversible cyclic voltammetric responses due to $Fc^{+}-Fc$ and Cu(II)−Cu(I) couples. The ready accessibility of the redox potentials makes these complexes efficient multifunctional model chemical nucleases showing plasmid DNA cleavage activity in the presence of both oxidizing and reducing agents, involving the Fc moiety and Cu(II) center for their activity, forming reactive hydroxyl radicals. The complexes show efficient DNA photocleavage activity in visible light of different wavelengths including red light of 647 nm. Although the Fc-tpy and Ph-tpy complexes of the dppz ligand have similar DNA binding affinity, the Fc-tpy complex **3** shows significantly better DNA photocleavage activity than the Ph-tpy complex **4**. The DNA photocleavage reactions follow a hydroxyl radical pathway. The spectral studies reveal photo-oxidation of the ferrocene moiety, forming a reactive ferrocenium species that possibly degrades, making the complexes significantly more reactive than its reported analogue having a $FcCH_2N(CH_2Py)_2$ ligand.[39] The ferrocenyl moiety in **3** shows enhanced cellular activity in HeLa cancer cells over its phenyl analogue in a similar way, as is known for ferrocifen over tamoxifen. The results are of importance toward developing the unexplored chemistry of bioorganometallic complexes as metal-based photoactivated anticancer agents showing DNA cleavage activity within the phototherapeutic spectral window.

Experimental Section

Materials and Methods. All reagents and chemicals were procured from commercial sources. Ferrocene carboxaldehyde, 2-acetylpyridine, calf thymus (CT)-DNA, agarose (molecular biology grade), ethidium bromide, distamycin-A, methyl green, and catalase were purchased from Sigma-Aldrich (USA). The supercoiled (SC) pUC19 DNA (cesium chloride purified) was obtained from Bangalore Genie (India). Tris(hydroxymethyl)-aminomethane−HCl (Tris−HCl) buffer was prepared by using deionized and double distilled water. 4′-Ferrocenyl-2,2′:6′,2″-terpyridine (Fc-tpy), 4′-phenyl-2,2′:6′,2″-terpyridine (Ph-tpy), dipyrido[3,2-*d*:2′,3′-*f*]quinoxaline (dpq), and dipyrido[3,2-*a*:2′,3′-*c*]phenazine (dppz) were prepared following literature procedures.[54−56] The solvents were purified using standard procedures.[57] The complexes were prepared under inert atmosphere.

A Thermo Finnigan FLASH EA 1112 CHNS analyzer was used for elemental analysis. The infrared and electronic spectra were recorded on PerkinElmer Lambda 35 and Cary 300 bio UV−visible spectrometers, respectively. Magnetic susceptibility data at 298 K for the powdered samples of the complexes were obtained from a model 300 Lewis-coil force magnetometer, George Associates Inc. (Berkeley, CA) using $Hg[Co(NCS)_4]$ as standard. Diamagnetic corrections were done on the experimental susceptibility data.[58] Molar conductivity measurements were made using a Control Dynamics (India) conductivity meter. Cyclic voltammetric measurements were carried out at room temperature on an EG&G PAR 253 VersaStat potentiostat/galvanostat using a three-electrode configuration consisting of a glassy carbon working, platinum wire auxiliary, and saturated calomel reference (SCE) electrode. Ferrocene (E_f = 0.41 V) was used as a standard in aqueous DMF (30%)−0.1 M KCl. Electrospray ionization mass spectral measurements were made using a Bruker Daltonics Esquire 300 Plus ESI model. A UV-A lamp of 365 nm (6 W) was used for UV photolysis experiments.

Synthesis of $[Cu(Fc\text{-}tpy)(B)](ClO_4)_2$ (B = phen, 1; dpq, 2; dppz, 3). Complexes **1**−**3** were prepared by following a general synthetic procedure in which a methanolic solution (5 mL) of $Cu(NO_3)_2\cdot 2H_2O$ (0.12 g, 0.5 mmol) was initially reacted with the terpyridyl ligand (Fc-tpy, 0.21 g, 0.5 mmol) dissolved in a methanol−chloroform mixture (4:1 v/v, 10 mL), and the resulting solution was stirred for 1 h under dark conditions followed by cooling in

(52) Delaey, E.; Van Larr, F.; De Vos, D.; Kamuhabwa, A.; Jacobs, P.; De Witte, P. *J. Photochem. Photobiol., B* **2000**, *55*, 27–36.
(53) Kang, H. C.; Kim, I.-J.; Park, H.-W.; Jang, S.-G.; Ahn, S.-A.; Yoon, S. N.; Chang, W. J.; Yoo, B. C.; Park, J.-G. *Cancer Lett.* **2007**, *247*, 40–47.
(54) (a) Constable, E. C.; Edwards, A. J.; Martínez-Máñez, R.; Raithby, P. R.; Thompson, A. M. W. C. *J. Chem. Soc., Dalton Trans.* **1994**, 645–650. (b) Moya, S. A.; Pastene, R.; Bozec, H. L.; Baricelli, P. J.; Pardey, A. J.; Gimeno, J. *Inorg. Chim. Acta* **2001**, *312*, 7–14.
(55) Collins, J. G.; Sleeman, A. D.; Aldrich, J. R.; Greguric, I.; Hambly, T. W. *Inorg. Chem.* **1998**, *37*, 3133–3141.
(56) Amouyal, E.; Homsi, A.; Chambron, J.-C.; Sauvage, J. P. *J. Chem. Soc., Dalton Trans.* **1990**, 1841–1845.
(57) Perrin, D. D.; Armarego, W. L. F.; Perrin, D. R. *Purification of Laboratory Chemicals*; Pergamon Press: Oxford, 1980.
(58) Kahn, O. *Molecular Magnetism*; VCH: Weinheim, 1993.

an ice bath. To the ice-cold solution was added a methanolic solution (10 mL) of the heterocyclic base B (phen, 0.1 g; dpq, 0.12 g; dppz, 0.14 g; 0.5 mmol) with continuous stirring for 1 h. Subsequently, a methanolic solution of $NaClO_4$ (0.12 g, 1.0 mmol) was added, and the solution was stirred for a further 15 min. The solid thus obtained was isolated as the perchlorate salt, washed with cold methanol, and dried under vacuum over P_4O_{10} (yield: 0.35 g, ~80% for **1**; 0.35 g, ~75% for **2**; 0.34 mg, ~60% for **3**).

Anal. Calcd for $C_{37}H_{27}Cl_2CuFeN_5O_8$ (**1**): C, 51.68; H, 3.16; N, 8.14. Found: C, 51.45; H, 2.99; N, 8.29. FT-IR (KBr phase): 3466br, 3078w, 1609s, 1572w, 1552w, 1522w, 1497w, 1477m, 1432m, 1254w, 1149m, 1095vs (ClO_4^-), 1022w, 847m, 793m, 721m, 624s, 516w cm^{-1} (br, broad; vs, very strong; s, strong; m, medium; w, weak). ESI-MS in MeCN: m/z 330 $[M - 2ClO_4]^{2+}$. UV−visible in aqueous DMF (15% DMF) [λ_{max}, nm (ε, M^{-1} cm^{-1})]: 267 (49 140), 287 (36 780), 327 (23 800), 340 (21 110), 410 (1720), 545 (3225). Λ_M, S m^2 M^{-1} in DMF at 25 °C: 133.

Anal. Calcd for $C_{39}H_{27}Cl_2CuFeN_7O_8$ (**2**): C, 51.36; H, 2.98; N, 10.75. Found: C, 51.08; H, 3.23; N, 10.59. FT-IR (KBr phase): 3446w(br), 3082w, 1607s, 1570w, 1552w, 1497w, 1474s, 1434m, 1405w, 1386w, 1254w, 1088vs (ClO_4^-), 820w, 790m, 736w, 624s, 516w cm^{-1}. ESI-MS in MeCN: m/z 356 $[M - 2ClO_4]^{2+}$. UV−visible in aqueous DMF (15% DMF) [λ_{max}, nm (ε, M^{-1} cm^{-1})]: 257 (48 430), 289 (40 000), 327 (25 620), 340 (22 530), 411 (1710), 546 (3030). Λ_M, S m^2 M^{-1} in DMF at 25 °C: 137.

Anal. Calcd for $C_{43}H_{29}Cl_2CuFeN_7O_8$ (**3**): C, 53.68; H, 3.04; N, 10.19. Found: C, 53.44; H, 3.26; N, 10.30. FT-IR (KBr phase): 3469w(br), 3082w, 1608s, 1568w, 1554w, 1495m, 1476m, 1434w, 1359w, 1254w, 1090vs (ClO_4^-), 822w, 790w, 771w, 737w, 623s, 516w cm^{-1}. ESI-MS in MeCN: m/z 381 $[M - 2ClO_4]^{2+}$. UV−visible in aqueous DMF (15% DMF) [λ_{max}, nm, (ε, M^{-1} cm^{-1})]: 272 (67 200), 287 (54 810), 327 (31 870), 340 (29 580), 361 (14 130), 380 (12 290), 413 (2060), 546 (3760). Λ_M, S m^2 M^{-1} in DMF at 25 °C: 134.

Synthesis of [Cu(Ph-tpy)(dppz)](ClO$_4$)$_2$ (4). A methanolic solution (15 mL) of Ph-tpy ligand (0.15 g, 0.5 mmol) was added to $Cu(ClO_4)_2 \cdot 6H_2O$ (0.5 mmol, 0.19 g) in methanol (10 mL), and the resulting solution was stirred for 45 min followed by cooling in an ice bath. To the cold solution was added a methanolic solution (15 mL) of dppz (0.14 g; 0.5 mmol) with continuous stirring for 2 h. The solid thus formed was collected, isolated, washed with cold methanol, and finally dried under vacuum over P_4O_{10} (yield: 0.27 g, 65%). Anal. Calcd for $C_{39}H_{25}Cl_2CuN_7O_8$ (**4**): C, 53.03; H, 3.10; N, 9.37. Found: C, 52.83; H, 3.31; N, 9.19. FT-IR (KBr phase): 3533w(br), 3076w, 1611s, 1558w, 1572w, 1492m, 1477m, 1419m, 1360m, 1249w, 1094vs (ClO_4^-), 819w, 794w, 766m, 733m, 623m cm^{-1}. ESI-MS in MeCN: m/z 241 $[M - 2ClO_4]^{2+}$. UV−visible in aqueous DMF (15% DMF) [λ_{max}, nm (ε, M^{-1} cm^{-1})]: 272 (70 950), 287 (55 500), 327 (20 930), 346 (19 450), 360 (13 800), 380 (12 280), 433 (215), 640 (80). Λ_M, S m^2 M^{-1} in DMF at 25 °C: 146.

CAUTION! *Perchlorate salts are potentially explosive; only a small quantity of the complex was handled with precautions.*

X-ray Crystallographic Procedure. Single crystals of the PF_6 salt of the phenanthroline complex **1** and dipyridophenazine complex **3** were obtained by slow evaporation of the MeCN solution of the complexes prepared from the nitrate salts. The X-ray intensity data were collected on a Bruker Smart Kappa APEX II CCD area detector with a fine-focused sealed tube with graphite-monochromated Mo Kα (λ = 0.71073 Å) radiation at 293 K using a ω-scan mode. Empirical absorption corrections were made using a multiscan program.[59] The structure was solved by the direct method and refined by full matrix least-squares on F^2 (SHELX-97).[60] The non-hydrogen atoms were refined with anisotropic thermal parameters, while the hydrogen atoms were fixed geometrically and allowed to refine using a riding model. Detailed crystallographic parameters are given in Table S1 (see Supporting Information). Selected crystal data for $[Cu(Fc\text{-}tpy)(phen)](PF_6)_2$: $C_{37}H_{27}CuF_{12}FeN_5P_2$, M = 950.97, monoclinic $C2/c$, a = 28.524(7) Å, b = 9.382(2) Å, c = 29.117(7) Å, $\alpha = \gamma = 90.0°$, β = 110.783(4)°, V = 7285(3) $Å^3$, Z = 8, ρ_{calcd} = 1.734 g cm^{-3}, T = 293(2) K, μ = 1.169 mm^{-1}, GOOF = 1.022, $R_1(wR_2)$ = 0.0821 (0.1677) for 8717 reflections with $I > 2\sigma(I)$ and 526 parameters [$R_1(F^2)$ = 0.1624 (all data)]. Selected crystal data for $[Cu(Fc\text{-}tpy)(dppz)](PF_6)_2 \cdot CH_3CN$: $C_{45}H_{32}CuF_{12}FeN_8P_2$, M = 1094.12, triclinic $P\bar{1}$, a = 12.3970(9) Å, b = 12.7771(10) Å, c = 15.3816(11) Å, α = 66.581(4)°, β = 87.760(4)°, γ = 85.033(4)°, V = 2227.3(3) $Å^3$, Z = 2, ρ_{calcd} = 1.631 g cm^{-3}, T = 293(2) K, μ = 0.970 mm^{-1}, GOOF = 1.055, R_1 (wR_2) = 0.0539 (0.1485) for 13 109 reflections with $I > 2\sigma(I)$ and 622 parameters [$R_1(F^2)$ = 0.1182 (all data)]. The perspective views of the complexes were obtained using ORTEP-3 for windows.[61]

DNA Binding Experiments. The experiments were carried out using CT-DNA in 5 mM of Tris−HCl or phosphate buffer medium. The purity of the CT-DNA was verified by taking the ratio of the absorbance values at 260 and 280 nm in the respective buffer, which was found to be 1.9:1, indicating the absence of any protein impurities in the DNA sample. The molar absorption coefficient (6600 M^{-1} cm^{-1}) of CT-DNA at 260 nm was used to determine the CT-DNA concentration.[62] The UV−visible absorption titration experiments were carried out in 5 mM Tris−HCl buffer with a fixed complex concentration (20 μM). An equal quantity of DNA was added during titration to both reference and sample solution. The spectra were recorded after 5 min, allowing the complexes to bind to the DNA. The intrinsic equilibrium binding constant (K_b) and the binding site size (s, b.p.) of the complexes to CT-DNA were obtained from a nonlinear fit of the absorption data by the McGhee−von Hippel method using the equation of Bard and co-workers: $\Delta\varepsilon_{af}/\Delta\varepsilon_{bf} = (b - (b^2 - 2K_b^2C_t[DNA]/s)^{1/2})/2K_b$, where $b = 1 + K_bC_t + K_b[DNA]/2s$; C_t is the total concentration of the metal complex; s is the binding site size (in base pairs) of the metal complex interacting with the DNA; ε_f, ε_a, and ε_b are respectively the molar extinction coefficient values of the free complex in solution, complex bound to DNA at a definite concentration, and the complex in completely bound form with CT-DNA.[63] In DNA melting experiments, the absorbance intensity of CT-DNA (160 μM) in 5 mM phosphate buffer (pH 6.8) containing 2% DMF was measured at 260 nm by varying the temperature from 40 to 90 °C at a scan rate of 0.5 °C min^{-1} both in the absence and in the presence of the complexes (20 μM). The melting temperatures (T_m) were calculated from the maxima of the first derivative of the melting plot. Viscosity measurements were performed in a Schott Gerate AVS310 automated viscometer fixed with a thermostatic bath at a constant temperature of 37(±0.1) °C. A 3 mL quantity of the DNA solution (150 μM) in 5 mM Tris−HCl buffer medium was placed in the viscometer, and the titrations were carried out by adding 100 μL of the complexes from a stock solution of 500 μM in DMF. After each addition, the solution was carefully mixed, the flow time was measured three times to an accuracy of 0.3 s with the automated timer, and an average time was calculated. The flow time of the buffer alone was also measured. Relative specific viscosity of DNA, $(\eta/\eta_0)^{1/3}$, was plotted against [complex]/[DNA], where η and η_0 are the viscosity of DNA in the presence and absence of the complex. The viscosity values were calculated from the observed flow time of CT-DNA-containing solutions (t) duly corrected for that of the buffer alone (t_0), $\eta = (t - t_0)$.[64]

(59) Walker, N.; Stuart, D. *Acta Crystallogr.* **1983**, *A39*, 58–166.
(60) (a) Sheldrick, G. M. *SHELX-97, Programs for Crystal Structure Solution and Refinement*; University of Göttingen: Göttingen, Germany, 1997. (b) Sheldrick, G. M. *Acta Crystallogr.* **2008**, *A64*, 112–122.
(61) Johnson, C. K. *ORTEP-III*, Report ORNL-5138; Oak Ridge National Laboratory: Oak Ridge, TN, 1976.
(62) Reichman, M. E.; Rice, S. A.; Thomas, C. A.; Doty, P. *J. Am. Chem. Soc.* **1954**, *76*, 3047–3053.
(63) (a) McGhee, J. D.; Von Hippel, P. H. *J. Mol. Biol.* **1974**, *86*, 469–489. (b) Carter, M. T.; Rodriguez, M.; Bard, A. J. *J. Am. Chem. Soc.* **1989**, *111*, 8901–8911.
(64) Cohen, G.; Eisenberg, H. *Biopolymers* **1969**, *8*, 45–55.

DNA Cleavage Experiments. The experiments were carried out using SC pUC19 DNA (0.2 μg, 30 μM, 2686 base pairs) under aerobic conditions. Samples were prepared in the dark at 25 °C by taking 1 μL of SC DNA and 2 μL of the complexes from a stock solution in DMF followed by dilution in 50 mM Tris−HCl buffer (pH 7.2) containing 50 mM NaCl to make the total volume 20 μL. Photoinduced DNA cleavage experiments were done using visible light of 458, 568, and 647 nm wavelengths using a continuous-wave (CW) Ar−Kr laser (laser beam diameter = 1.8 mm, beam divergence = 0.70 mrad, Spectra Physics Water-Cooled Mixed-Gas Ion Laser Stabilite 2018-RM). The power of the laser beam was 50 mW, measured using Spectra Physics CW laser power meter (model 407A). The solution path length used for illumination in the glass vial was ~5 mm. The samples were incubated for 30 min before irradiation at 37 °C. Chemical nuclease experiments were carried out under dark conditions for 2 h incubation at 37 °C using a 10 μM complex solution in the presence of external agents such as hydrogen peroxide (250 μM) as an oxidizing agent and 3-mercaptopropionic acid (500 μM) as a reducing agent. To study the groove binding properties of the complexes, reactions were carried out in the presence of methyl green and distamycin-A as DNA major and minor groove blockers, respectively. Mechanistic investigations for the DNA photocleavage reactions were made in the presence of various external additives such as KI (500 μM), NaN_3 (500 μM), TEMP (500 μM), DMSO (4 μL), and catalase (8 units). After the DNA cleavage reaction, a 2 μL solution of loading dye containing 30 mM EDTA, 0.05% bromophenol blue, 0.05% xylene cyanol, and 36% glycerol was added to the reaction mixture. The electrophoresis was carried out on 1% agarose gel containing 1.0 μg mL^{-1} ethidium bromide in a dark room for 2 h at 45 V in 1X TAE (Tris-acetate-EDTA) buffer. The DNA cleavage products after the gel electrophoresis were visualized by UV light and photographed, and the band intensities were measured by using a UVITECH gel documentation system. Corrections were made for the low level of nicked circular (NC) form present in the original supercoiled (SC) DNA sample and for the low affinity of EB binding to the SC compared to the NC form of DNA.[65] The observed error in measuring the band intensities was ~5%.

Cell Cytotoxicity Experiments. The cytotoxicity experiments of the dppz complexes **3** and **4** toward HeLa cells were carried out by the MTT (3-(4,5-dimethylthiazol-2-yl)-2,5-diphenyltetrazolium bromide) assay, which is based on the cleavage of tetrazolium rings of MTT by mitochondrial dehydrogenases in the viable cells to dark blue membrane impermeable crystals of formazan, which can be quantified at 595 nm on solubilization in DMSO, giving a measure of the number of viable cells.[66] Human cervical carcinoma HeLa cells (~8000) were taken in a 96-well culture plate in DMEM containing 10% FBS and incubated for 24 h at 37 °C in a CO_2 incubator, followed by the addition of the complex solution in 10% FBS buffer containing 1% DMSO. After 3 h incubation under dark conditions, the medium was replaced by fresh PBS buffer, and the culture plate was kept inside the Luzchem photoreactor (model LZC-1, Ontario, Canada) fitted with eight Sylvania fluorescent white tubes with a fluence rate of 2.4 mW cm^{-2} to provide a total dose of 10 J cm^{-2} for photoirradiation with 400−700 nm visible light. After 45 min photoexposure, PBS medium was replaced by DMEM−10% FBS and further incubated for 24 h in the dark. Thereafter, a 25 μL portion of 5 mg mL^{-1} MTT was added to each well and incubated for an additional 3 h. The culture medium was discarded, 200 μL of DMSO was added to dissolve the formazan crystals formed, and the absorbance at 595 nm was determined with a BIORAD ELISA plate reader. The percentage ratio of the absorbance of the treated cells to the untreated controls gave the measurement of cytotoxicity. The IC_{50} values were determined by nonlinear regression analysis (GraphPad Prism 5.0).

Acknowledgment. We thank the Department of Science and Technology (DST), Government of India, and the Council of Scientific and Industrial Research (CSIR), New Delhi, for financial support (SR/S5/MBD-02/2007 and 01(2018)/06/EMR-II). We are thankful to DST for the CCD diffractometer facility and the Alexander von Humboldt Foundation, Germany, for donation of an electroanalytical system. B.B. is thankful to the CSIR, New Delhi, for a research fellowship. A.R.C. thanks DST for a J. C. Bose National Fellowship.

Supporting Information Available: CIF files giving crystallographic data for the complexes **1a** and **3a**·MeCN, detailed crystallographic data (Table S1) and figures showing ESI mass spectra (Figures S1−S4), IR spectra (Figures S5−S8), UV−visible spectra (Figure S9), cyclic voltammograms (Figure S11), unit cell packing and stacking diagrams (Figures S12−S16), DNA binding plots (Figure S17), bar diagram of chemical nuclease activity (Figure S18), gel electrophoresis diagrams (Figures S19−20), UV−visible spectral titration plots (Figure S21), and MTT assay for controls (Figure S22). This material is available free of charge via the Internet at http://pubs.acs.org.

(65) Bernadou, J.; Pratviel, G.; Bennis, F.; Girardet, M.; Meunier, B. *Biochemistry* **1989**, *28*, 7268–7275.
(66) Mosmann, T. *J. Immunol. Methods* **1983**, *65*, 55–63.